LUND UNIVERSITY
Faculty of Science

Review of DM searches in the ATLAS and LDMX experiments

Disa Gustafsson

Thesis submitted for bachelor's degree

Project duration: 6 months
Examination: Spring 2020

Supervised by Caterina Doglioni and Ruth Pöttgen

Department of Physics
Division of Particle Physics
June, 2020

Abstract

Several findings show that dark matter makes up 27% of the universe. The goals of this thesis are to understand some of the most important evidences and candidates for dark matter, as well as how dark matter is searched for. The ATLAS and LDMX experiments are reviewed to give a greater insight into the search for dark matter. Two papers from ATLAS are studied more carefully and the data from these were re-plotted using a Jupyter Notebook to understand how the data is analyzed. Comparing the ATLAS and LDMX experiments show that their respective method and targeted models differ. LDMX is optimized for studying a specific signature, while ATLAS explores many different final states. Both experiments search for mediators between dark matter and standard model matter, using different collision methods and energy ranges. LDMX is a fixed-target experiment and will cover lower interaction strengths than possible before, while ATLAS is a collision experiment connected to the worlds most powerful accelerator. Finally, both experiments will continue to improve during the upcoming years.

Acknowledgements

I wish to thank my supervisors, Caterina and Ruth, for giving great support and explanations and for being great role models, throughout my thesis work and years at the university.

Contents

List of Abbreviations

DM = Dark Matter
SM = Standard Model
LHC = Large Hadron Collider
LDMX = a Light Dark Matter eXperiment
SLAC = Stanford Linear Accelerator Center
QCD = Quantum Chromodynamics
QED = Quantum Electrodynamics
COM = Centre Of Mass
TLA = Trigger-object Level Analysis
EOT = Electrons On Target

Chapter 1

Introduction

The Standard Model of Particle Physics - SM - contains the fundamental particles and interactions that are known as of today. These make up the ordinary, so-called baryonic matter. However, the SM is not complete and can not explain all physical phenomena. One phenomenon that remains unexplained is Dark Matter - DM -, which seems to make up 27 % of the matter-energy in the universe. Discovering the possible particle nature of DM would give a greater understanding of the composition of the universe and how galaxies are held together [1]. A more complete Standard Model could also describe other experimental results further, and help develop new theories within physics.

The goals of this thesis are to understand some of the most important evidences and candidates for dark matter, as well as how dark matter is searched for. This will be done through first describing the theoretical and experimental background of DM, containing evidence for the existence of DM, different models for DM candidates as well as how to search for DM. After this, two experiments looking for DM (among with other physics phenomena) will be reviewed. First, proton-proton collisions at the ATLAS detector at CERN [2] and second, electro-nuclear fixed-target collisions at LDMX - a Light Dark Matter eXperiment-, which will be built at SLAC - Stanford Linear Accelerator Center- [3].

To further understand how the experimental data is analyzed to search for particles associated with dark matter, two experimental searches using different data-sets from ATLAS will be studied and compared, described in Ref. [4] and Ref. [5]. A Jupyter Notebook, [6] developed by a Lund student, will be used to reproduce part of the statistical analysis in the two papers.

Chapter 2

Theoretical and Experimental Background

2.1 The Standard Model

The Standard Model of Particle Physics - SM - describes the fundamental particles and interactions that are known as of today. Each particle in the SM is characterized by a mass, charge, and spin. These properties determine their respective categorization in the SM, which can be seen in Figure 2.1. The particles are divided into fermions and bosons. In the SM, a fermion has spin $\frac{1}{2}$ and obeys Fermi-Dirac statistics, whilst a boson has spin 0 or 1 and obeys Bose-Einstein statistics. All particles also have a corresponding antiparticle with opposite charge [7]. .

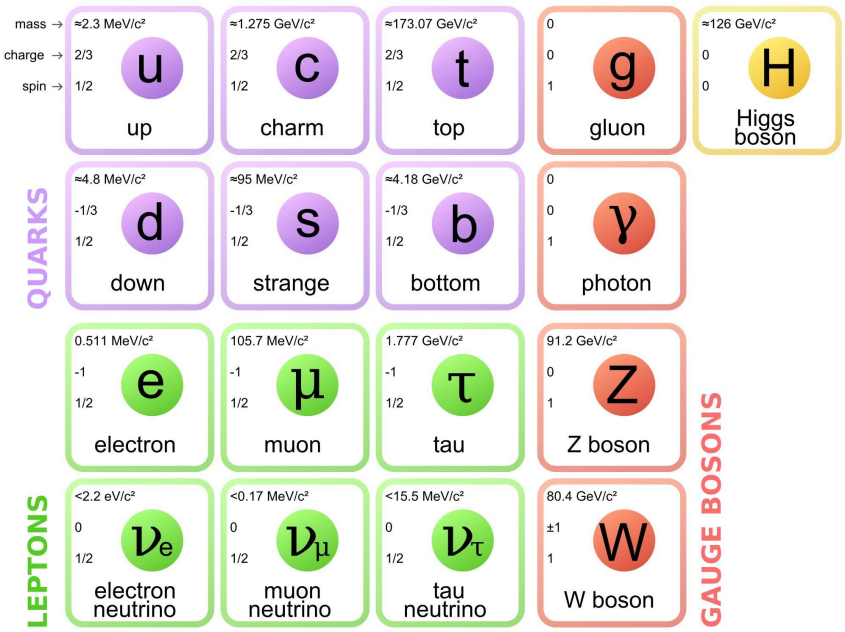

Figure 2.1: The fundamental particles in the Standard Model of Particle Physics [8].

The fermions are then divided into quarks and leptons. All quarks except the top quark can combine to make hadrons, for example mesons and baryons. A meson and baryon

consist of two and three quarks respectively. The fermions are also divided up into three generations, where the mass of the particles increases with the number of the generation [7].

The bosons are force mediators. The gluon mediates the strong force, the photon mediates the electromagnetic force and the Z and W mediate the weak force. Finally, the Higgs mechanism is responsible for the masses of most of the SM particles. A consequence of the Higgs mechanism is the presence of the Higgs boson [7].

Quantum Chromo Dynamics - QCD - and Quantum Electro Dynamics - QED - are the theories of the strong and electromagnetic interaction respectively. The gluon couples to color charge, which is carried by both quarks and gluons. The photon couples to electric charge, which is carried by any charged particle or hadron. In QED, the force becomes weaker with increased distance. However, in QCD the opposite holds. This can be compared with an elastic band - when pulling the band the force becomes stronger and when compressing the band the force becomes less strong. A consequence of this is that quarks in hadrons behave like free particles (asymptotic freedom), but when increasing the distance between the quarks it becomes difficult to isolate the quarks from the hadron (confinement) [7].

The SM is not complete and there are several beyond SM problems, where DM is one of the unanswered questions [7].

2.1.1 Jets

Hadronization is the process in which gluon and quarks combine to form hadrons, that occurs as a consequence of asymptotic freedom and confinement [7]. The result of this process can be grouped into jets, using jet algorithms [4]. A jet can be visualized as a collimated cone of particles all located in a similar location in the detector. The four-momentum of the jet is the sum of the four-momenta of the constituents of the jet [7].

2.2 The existence of DM

2.2.1 Evidence from early observations

Several findings indicate the existence of DM. One classical observation is the movement of galaxy clusters. In 1930, the Swedish astronomer Lundmark noticed that the predicted relationship of how much mass there is in a luminous galaxy was not correct. He calculated that there had to exist more mass as the galaxies were rotating with a speed such that the gravity generated by the luminous mass in the galaxy could not hold them together [9]. However, most famous for the discovery is the Swiss astronomer Zwicky who also observed this three years later [10]. He studied the Coma cluster of galaxies and calculated that there had to exist two orders of magnitude more mass. Around this time, the Dutch astronomer Oort also noticed that the stars in our galaxy were moving faster than the gravity generated by their visible matter would allow [9]. Another observation confirming the need for more matter than what was visible was in the rotation curves of spiral galaxies. It was in the 1970s that the discussion of "the missing mass problem" really started, when Rubin and Ford measured the rotational velocity of the galaxy Andromeda

Nebula. They detected that the rotational velocity did not decrease with the radius as expected. Instead, the rotation curve flattened out, meaning that the hydrogen clouds and stars further out from the center of the galaxy had an almost constant rotational velocity (see Figure 2.2). To summarize, they all concluded that there had to exist more mass than just what was visible, for the laws of physics to hold [9].

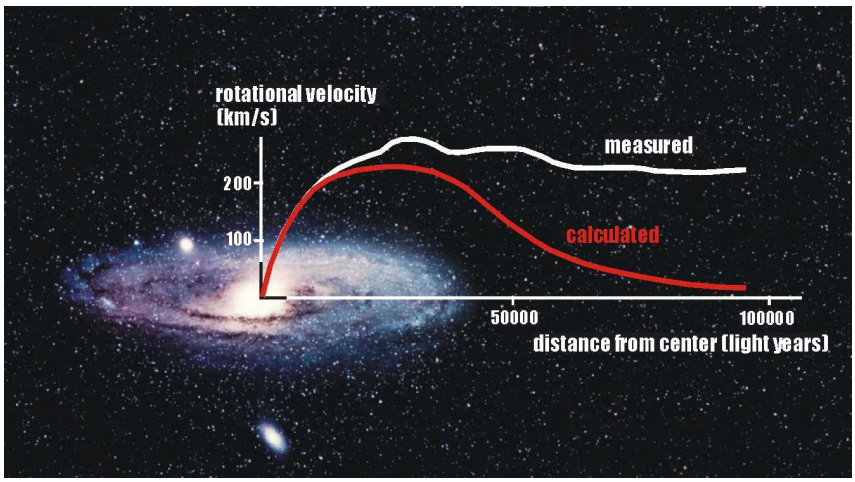

Figure 2.2: The rotational velocity of a galaxy as a function of the distance from its center [9].

2.2.2 Evidence from microlensing

Einstein's general theory of relativity predicts that the gravitational field around massive objects will be bent due to the distortion of space and time. This means that a massive object will bend and distort light from any source behind it in the same line of sight. This effect is called gravitational lensing [11]. The result of this effect is that if a massive object is in between the same line of sight as an observer and the studied object, then the observer will see a magnified image of the studied object (see Figure 2.3). Gravitational microlensing is the same phenomenon, but with less massive objects, for example a star, bending the light [11].

The position of the light source relative to the massive object determines how strong the lensing effect is. The lensing can, for example, be weak or strong. If the source and object are perfectly aligned then the lensing will be strong and an "Einstein ring", as seen in Figure 2.4, will be seen [11].

Gravitational lensing can be used to map out mass distributions in the galaxy, as the observed light is dependent on the mass distribution [11]. The EROS-2 Survey used gravitational microlensing to search for MACHOS, MAssive Compact Halo Objects, in 2007 [13]. They observed 7 million stars but found only one of these was a candidate for gravitational lensing, which indicates that most of the mass distribution of the universe causing gravitational lensing is not visible or baryonic [13].

Another indication of the existence of DM is the Bullet Cluster (see Figure 2.5) detected in 1998. The Bullet Cluster has formed from a collision between two galaxy clusters.

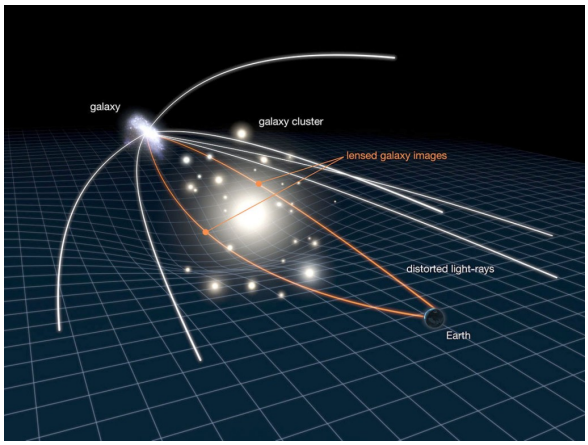

Figure 2.3: Light bend by a massive object, causing gravitational lensing [12].

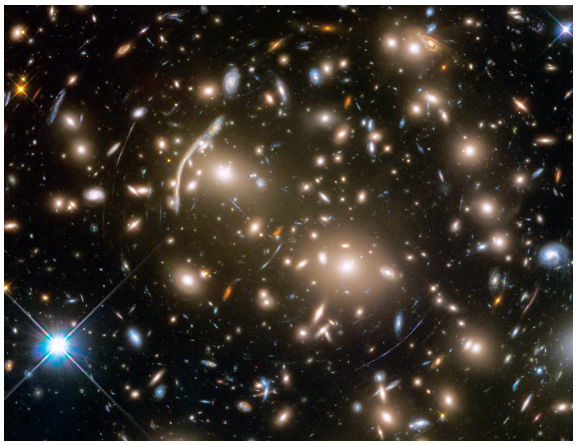

Figure 2.4: Einstein Rings [11].

Using microlensing, it was possible to see that the visible baryonic part and non-baryonic part had separated after the collision. The red part, seen in Figure 2.5, was concluded to be baryonic matter, while the blue, non-baryonic part was concluded to be DM. It was observed that the baryonic matter obtained its shape after the collision, unlike the DM, which had not interacted in the same way, meaning that DM behaves like a collisionless fluid and only has a limited amount of self-interactions, if any [14].

Figure 2.5: The Bullet Cluster, a collision between two galaxy clusters [9].

2.2.3 Evidence from the early universe

As the universe today is expanding, the early universe must have been compressed. Compressing a gas makes it warmer as the energy is conserved. Similarly, the universe in its first seconds must have been extremely warm and compact [15].

Directly after the Big Bang, the universe expanded and cooled rapidly. This period is called *inflation* [16]. The universe at this time consisted of a warm, photon-emitting gas of ionized matter, where disturbances are believed to have propagated as sound waves. A compression would heat this gas and a rarefaction would cool it [17].

About one second after the Big Bang, one theory is that the universe, when expanding, went from being in local thermal equilibrium, to particles falling out of this equilibrium, (as the Hubble expansion rate became larger than the interaction rate). This is referred to as the *freeze-out* [18].

The universe at this point had also become cool enough for protons and neutrons to fuse. This fusion is called the Big Bang Nucleosynthesis - BBN - and it lasted up to a few minutes after the Big Bang. About 380 000 years later, protons and neutrons started combining with electrons, causing neutral hydrogen to form. This made it possible for photons to travel freely, as the photons now could decouple from the charge-neutral atoms. The expansion also decreased the effective temperature of the photons to around 2.7 K. It is these photons that make up the Cosmic Background Radiation - CMB - today [15]. Studies of the BBN and CMB allow us to get an insight into the early universe and give evidence for the amount of DM today as discussed in the next sections.

The Big Bang Nucleosynthesis

During the BBN, light elements, for example, H, ^{2}H, He, and Li were formed. Today, ^{2}H is formed in stars. However, most of the ^{2}H fuses to ^{4}He, meaning that the ^{2}H from the BBN still makes up most of the ^{2}H in the universe [13].

It is possible to estimate the H to ^{2}H ratio after the BBN through studying unchanged areas in the universe consisting of light elements. This ratio depends on the overall density of baryons, $\Omega_b h^2$. In general, Ω is a matter density relative to a reference density, and h^2 is the reduced Hubble constant. Here, Ω_b is the baryonic matter density. Through measuring the H to ^{2}H ratio, the baryonic matter density is calculated to be about 20% of the total matter in the universe [13].

The Cosmic Background Radiation

The small temperature fluctuations of the CMB are due to compressions and rarefactions in the gas of the early universe mentioned above [17]. As warmer, denser areas had a stronger gravity pull and attracted more matter, the fluctuations are also dependent on the number of baryons at the time of the early universe [13]. But the baryons did not have a gravitational pull strong enough to form galaxies. Hence, the number of baryons must be linked to the amount of DM [19]. Before the photons decoupled, they held the baryons together. After this, it is believed that baryons were attracted to the DM and together could form galaxies [19]. This theory of galaxy formation has been tested using simulations on supercomputers [20].

The CMB radiation can be measured, and from that, the amount of matter in the universe can be determined. A CMB telescope measures different voltages, where a higher voltage indicates a stronger incident radiation and a warmer CMB temperature [15]. Studying the power spectrum, where the CMB temperature fluctuations are plotted against different angular scales on the sky, makes it possible to determine the structure and composition of the universe [16]. Comparing the size of the bumps in a power spectrum within a given theory makes it possible to estimate that DM constitutes around 27 % of the universe [16].

2.3 DM Candidates

From the studies of galaxy clusters, the rotation curves of spiral galaxies, and the effects DM has on light, it is established that DM is non-baryonic, massive, and interacts gravitationally. The mass of DM particles can be anywhere in the order from 10^{-20} eV to several solar masses, depending on the origin of DM. It is also acknowledged that DM is stable on a cosmological timescale, through studying the CMB and tracing back DM to the early universe [21]. Finally, it is known that DM does not interact electromagnetically as it is not visible [22]. In the following, I will describe some of the most common DM candidates and their properties.

2.3.1 Hot and Cold DM

Hot dark matter, HDM, corresponds to particles with a small mass, traveling at relativistic velocities (for example neutrinos). If DM is hot, fast traveling HDM could escape the small density fluctuations in the early universe, which would have decreased these fluctuations. Galaxies would then have been formed slower and later in the history of the universe. This is not what is seen today, meaning that DM can not be hot [19].

Instead, DM candidates today are believed to be cold. Cold Dark Matter, CDM, corresponds to particles with a mass around 1 GeV, traveling slow. Warm Dark Matter is a mixture of Hot and Cold DM. Using simulations on supercomputers as mentioned above, galaxy formations using these different types of DM can be tested. Fig. 2.6 shows simulations of what Hot, Warm, and Cold DM would look like in the early universe, and today. It is seen that Cold DM is most consistent with how the universe looks like [19].

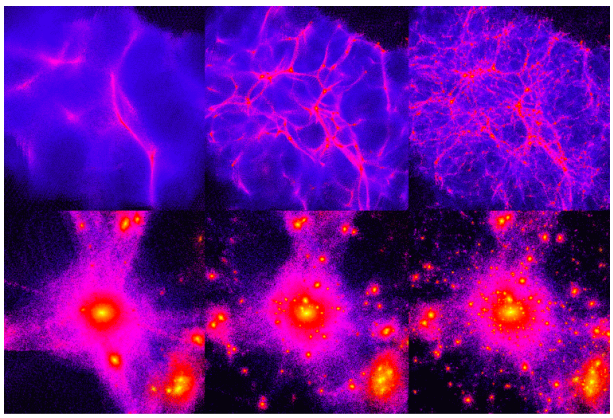

Figure 2.6: Simulations of what Hot, Warm and respective Cold DM would look like (left to right) in the early universe respective today (top to bottom) [19].

2.3.2 DM as Thermal Relics

One theory is that the amount of DM became constant after freeze-out in the early universe. In this theory, DM and SM particles were in equilibrium before the freeze-out. When the universe cooled and DM fell out of equilibrium, the amount of DM became

constant. These theorized DM particles are called thermal relics, and the density of the thermal relic DM is called the thermal relic density [23].

Below, different theoretical models describing thermal relic candidates for DM and their non-gravitational interaction with SM, are described. Several of these models, such as WIMPs and light dark matter, are motivated as they agree with the thermal relic density existent in the universe [21].

WIMPs and Super Symmetry Particles

One theory is that DM particles are Weakly Interactive Massive Particles - WIMPs -, meaning that the mediator between DM and SM is a weak boson or a particle similar to that, and that the DM particles would have a mass in the GeV to TeV range [24].

One type of WIMP is Super Symmetric particles. In Supersymmetry, all the fundamental particles have a super symmetric partner, which differs in mass and by half an integer spin. The lightest supersymmetric particle is a DM candidate, as it is believed to interact weakly, not electromagnetically, and have a long lifetime [25].

WIMPs can not be lighter than a few GeV - the annihilation into SM particles via a heavy mediator would then be inefficient. In theoretical models for lighter DM, another force mediator is needed [21].

The Dark Photon as mediator of DM

For light DM - LDM - (which is in the MeV to GeV range) to interact with SM, a light force mediator is needed. One theory is that the dark photon, is this force mediator, A' (seen in Fig. 2.7 and Fig. 2.8). The dark photon would have spin 1 and a non-zero mass, unlike the photon [21].

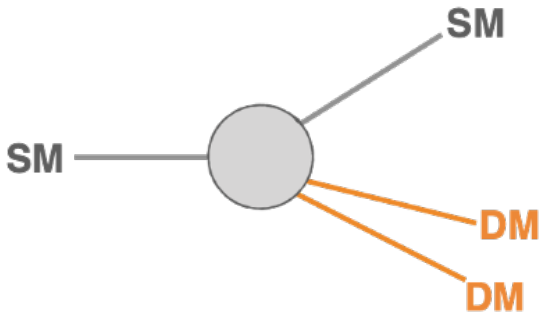

Figure 2.7: DM production from scattering of SM particles [21].

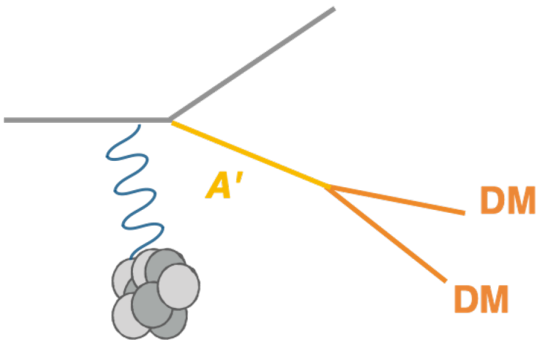

Figure 2.8: DM production from scattering of SM particles. Shown with the force mediator A' [21].

The Z' boson as mediator of DM

Another model for DM is that a new Z' boson is the force mediator between SM and DM. The Z' is more massive than the Z boson, around 500 GeV $\leq m_{Z'} \leq$4 TeV, with spin 1. The Z' boson in certain theories is also leptophobic, meaning that it does not couple to leptons [26].

2.4 Searching for DM

Theoretical models, simulations, and experimental tools are all used to search for DM. Using theoretical models, as the DM candidates mentioned above, provides constraints on the experimental searches. Different theorized DM candidates exist in different energy ranges, which motivates DM experiments using various energies.

2.4.1 Experimental searches

There are several experimental methods to search for DM candidates experimentally: through direct and indirect detection experiments, colliders or, fixed-target experiments [24] [27]. Their complementarity for WIMPs can be seen in Fig. 2.9.

In direct and indirect detection experiments, DM is detected from or in space rather than produced. If the detection is indirect, SM particles produced from DM particle interactions are observed by telescopes. In direct detection, DM particles are observed directly when they interact with a detector on earth. In colliders and fixed-target experiments, on the other hand, normal matter particles are accelerated and collided in the hope of creating and detect DM particles [28]. If DM would be produced in a collider or fixed-target experiments, direct and indirect detection experiments would be used to confirm if the existence of the produced DM [29].

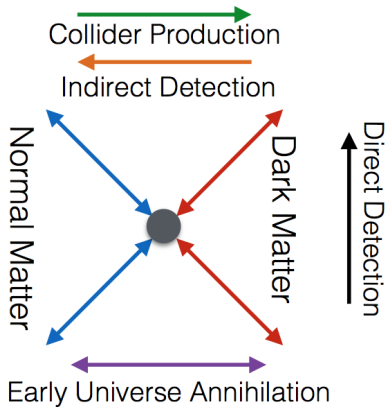

Figure 2.9: Possible ways for DM and SM particles to interact and be detected, compared to when DM particles were created in the early universe [27].

Chapter 3

ATLAS

3.1 The ATLAS experiment

ATLAS is a detector placed on one of the interaction points of the world's most powerful particle collider, LHC, at CERN. At LHC, proton beams are accelerated up to a center of mass energy of 13 TeV, with 7.5 TeV per beam, to collide [29]. ATLAS is used to study the outcome of these proton-proton (pp) collisions, and to search for new particles that could be DM or the associated mediators [5], [4].

To record the outcome of these collisions, an efficient layout detecting the events is needed. Further, as more data is produced than possible to handle at ATLAS, a trigger system is used to make a selection and only save the data from certain, selected types of events that are considered interesting. [30] ATLAS continues to develop, and by 2026, 10 times more data than today is expected to be delivered [29].

3.2 ATLAS layout

To record and identify the outcome of collided particles, particle detectors often consist of different layers, where the energy and momenta of the particles can be measured [7], [31].

ATLAS is composed of tracking detectors, an electromagnetic calorimeter (ECal), a hadronic calorimeter (HCal), and a muon spectrometer, seen in Fig. 3.1. The detector is covering the whole solid angle [4], so that very little escapes, which means that if there is any significant missing transverse momentum after the collision, the particles should not be detectable.

The tracking detector makes up the inner layer of the detector and consists of a magnet, which bends the particle's trajectory, and of silicon sensors that make it possible to measure the charge and momentum of the particle [7], [31].

After the tracking detector is first the electromagnetic calorimeter - ECal - and then the hadron calorimeter - HCal -. These consist of layers of active and passive material, where the particles interact in the passive material and the amount of deposited energy can be measured using the active material. The HCal consist of plastic scintillators as active material, and iron or steel as passive material. The ECal consists of the active

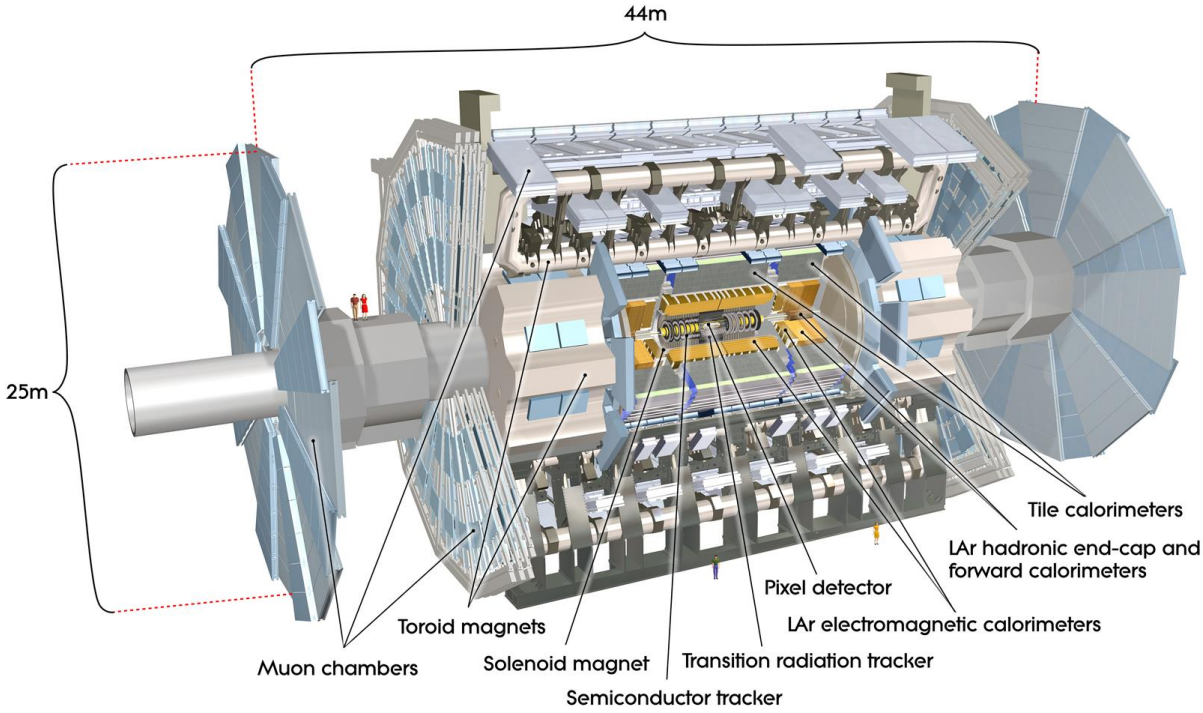

Figure 3.1: The ATLAS detector [32].

material, liquid argon, and the absorber material, lead. Electromagnetically charged particles and hadrons will leave a shower in the E- and HCal respectively, as they react either electromagnetically or strongly. Narrower, shorter showers can be seen in the ECal and longer, wider showers are seen in the HCal [7], [31].

Finally, the muon spectrometer is furthest out, as the muons travel through all previous detectors. Only muons leave a track in this detector [7], [31].

3.3 Overview of ATLAS searches searching for DM mediators

Two papers from ATLAS, Ref. [4] and Ref. [5], searching for new particles that could be the DM mediators, will be reviewed. The two papers describe searches for different theoretical models, including DM mediators in different energy ranges. Both searches use colliding protons at the LHC, and one exploits the trigger system in a non-standard way to save certain, selected data from the collisions. In both searches, when plotting the number of events vs. the invariant mass, an excess above the background would indicate the presence of a new resonant particle, which could be the mediators between DM and SM particles. No excesses were found in either analysis.

In this thesis, only the search for the Z' boson in Ref. [4] and Ref. [5] will be studied. Fig. 3.2 shows an example of how DM could be created when colliding protons, with the Z' boson as force mediator.

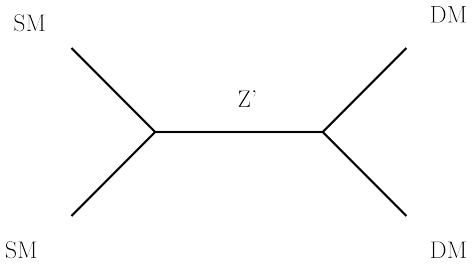

Figure 3.2: Diagram of a SM-DM interaction with Z' as the force mediator.

To search for the Z' boson decaying into DM, searches for invisible particles (missing momenta and missing energy) as well as a final dijet (two jet) state of two quarks (SM particles), are made. [22]. Fig. 3.3 show the production of a dijet- and an invisible DM final state, where g_q and g_{DM} are the coupling constants to quarks and DM respectively. The value of the coupling constant indicates the strength of the interaction [7], [31].

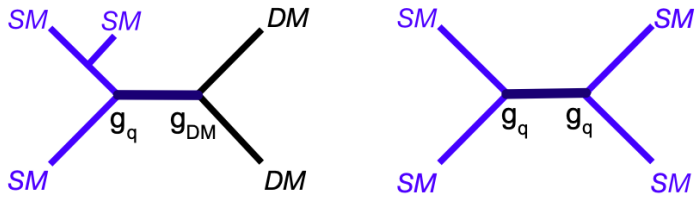

Figure 3.3: Left: Production of DM. Right: Production of a dijet final state. Sketch by Caterina Doglioni.

A data analysis from the Jupyter Notebook Ref. [6], with the method taken from Ref. [33] was used to reproduce the result starting from publicly available HEPData, Ref. [34] and Ref. [35]. The Jupyter Notebook was modified so that two different data sets could be plotted simultaneously.

First, the data and data selection of the searches will be outlined. Then, the backgrounds and the statistical analysis used in the searches and the Jupyter Notebook and will be described. Finally, the method from the Jupyter Notebook used to re-plot the result from the searches will be described.

3.3.1 Data

Parameters of the collided beams

The two papers studied, Ref. [4] and Ref. [5], both used pp - collisions at a COM energy, $\sqrt{s} = 13$ TeV. Study Ref. [4] searched for low mass dijet resonances in the mass range of 0.450-1.800 TeV, while study Ref. [5] searched for dijet resonances in the mass range 2-9 TeV.

The two studies used different amounts of data. The luminosity of a beam, L, depends on the characteristics of the accelerator and is a quantity that indicates the ability for a particle accelerator to produce a number of events in a given space and time. The luminosity multiplied by the total pp interaction cross-section σ, gives the collision rate.

The cross-section of a process σ is measured in barns (b) and is a measurement of how likely something is to occur. In particle physics, the cross-section can be a measurement of how likely it is for particles to collide and interact. The luminosity integrated over time, L_{int}, multiplied by the cross-section for a given process gives the total number of observed events. The unit for integrated luminosity is the inverse barn (b^{-1}) [36].

Search Ref. [4] used two datasets with different luminosities, while search Ref. [5] used one dataset,

Ref. [4]

- $L_{int} = 29.3$ fb^{-1}
- $L_{int} = 3.6$ fb^{-1}

Ref. [5]

- $L_{int} = 37$ fb^{-1}

Trigger level data and offline data

As mentioned in section 3.1, a trigger system is used to decide which events are saved to store and study further. An important parameter when selecting jets is the transverse momentum, p_T, of the jets. The transverse momentum is,

$$p_T = \sqrt{p_x^2 + p_y^2} \tag{3.1}$$

where $p_{x,y}$ are the momenta of the x and y direction respectively, and the z-axis is parallel to the incoming beams [37]. As the transverse momentum is conserved in the initial and final states of a collision, it is useful for identifying invisible particles.

In the ATLAS detector, there are two trigger systems used to select jets and record data, the L1 (First Level) and HLT (High Level Trigger) system. Only calorimeter triggers will be discussed in this thesis.

The L1 calorimeter trigger identifies jets, where the energy of the jet consists of the sum of energies deposited in a group of cells. The L1 trigger system can select events, for example, with one or multiple jets above a certain energy. The selected events are then passed to the HLT, which reconstructs them with more refined algorithms, mostly use calorimeter information. The jets reconstructed in this way are called trigger level jets. The triggers used in the two searches in this thesis select events based on the most energetic (leading) trigger jet. If the event is selected by the HLT, a more refined reconstruction can be performed on the CERN computer farm. Jets reconstructed in this way are called offline jets. The offline reconstruction is done in the same way as in the HLT, with the difference that the offline jets can be reconstructed using the entirety of the detector information [38], [39]. The ratio of the p_T of a jet reconstructed at the trigger-level or offline (called the jet p_T response) is less than 0.05% for lower masses, and negligible for masses of 1 TeV, meaning that the results from the trigger or the offline reconstruction are very similar.

In the two searches, only jets with the transverse momenta $p_T > 20$ GeV are used, to reduce the amount of data saved [5], [4].

Search Ref. [4] uses a new trigger level analysis - TLA -, and stores jets selected by the HLT, but only their four-momenta and calorimeter variables. Using this technique, less than 0.5% of the normal event size needs to be stored [4], [5].

Event selections

In the traditional dijet search, leading jets with a $p_T < 380$ GeV (which corresponds to dijet events of an invariant mass below about 1 TeV) are prescaled [4], meaning that only a small fraction of the generated events below this threshold passing the trigger are stored, the rest are discarded [4]. Jets with lower energies are chosen to be prescaled as the cross-section increases with lower energy (meaning the amount of data is higher at low energies) and as most LHC experiments study jets with higher energies.

Because the search Ref. [4] used a new TLA technique, less storage space for the selected events is needed, and prescaling is not necessary. This means that events with dijet masses below 1 TeV can be targeted.

The following leading- and subleading- jets were selected for the respective studies,

Ref. [4] $L = 29.3$ fb^{-1}
- Leading $p_T > 220$ GeV
- Subleading $p_T > 85$ GeV

Ref. [4] $L = 3.6$ fb^{-1}
- Leading $p_T > 185$ GeV
- Subleading $p_T > 85$ GeV

Ref. [5]
- Leading $p_T > 440$ GeV
- Subleading $p_T > 60$ GeV

Another parameter used to select events is the rapidity, y, which is defined as,

$$y = \frac{1}{2} \log \left[\frac{E + p_z}{E - p_z} \right] \tag{3.2}$$

where E and p_z are the beam's energy and momentum along the beam axis respectively. The pseudorapidity is the rapidity with the jet mass set to zero[1]. Even if the jet mass can not be measured in its entirety in ATLAS, the rapidity, instead of the pseudorapidity, is still used to select events, as it is a more precise option than setting the mass to zero. When searching for dijets, constraints are imposed on the rapidity difference between the two jets, y^*, where,

$$y^* = \frac{y_1 - y_2}{2} \tag{3.3}$$

where $y_{1,2}$ are rapidities of the respective highest and second highest p_T jets. This difference is invariant under Lorentz transformations along the beam axis, meaning that $y*$ is the rapidity of a dijet in the COM frame [40], [37], [4].

Different constraints are set on $|y*|$ to reduce the background, as signals have lower $|y*|$ values than the background [5]. The rapidity difference was set to,

Ref. [4]
- $|y^*| < 0.3$ for $m_{jj} > 450$ GeV
- $|y^*| < 0.6$ for 700 GeV $< m_{jj} <$ 1800 GeV

Ref. [5]
- $|y^*| < 0.6$
- $|y^*| < 1.2$ (not studied here)

[1]The four-vector can be represented using energy and three-momentum, but also using mass, energy and angles. The rapidity and pseudorapidity can be defined via these angles.

The $|y*| < 0.6$ constraint is applied for the Z' model, as the Z' boson model peaks at $|y*| = 0$.

3.3.2 Analysis

When searching for new particles, the number of events/bin (where a bin is a mass range) are plotted vs. the invariant mass (m_{jj}). The invariant mass is independent of the motion of the system and is defined as,

$$m_{jj} = \sqrt{(E_1 + E_2)^2 - (\vec{P_1} + \vec{P_2})^2} \tag{3.4}$$

where $E_{1,2}$ and $P_{1,2}$ is the energy and momentum of the respective first and second decay product [7].

The number of events/bin of the invariant mass distribution is plotted together with the estimated background (described below). A bump in the invariant mass distribution in data above the background could indicate that non-expected particles have been produced [4].

Distribution used for the searches

In the two searches, Ref. [4] and Ref. [5], the events selected are dijet events. From QCD, it is predicted that dijet events have a smoothly falling invariant mass distribution, and this was used to estimate the background distributions of the two searches.

In the two searches, the background was estimated by using a sliding-window fit (SWiFt) and a fit function. This background estimation technique fits the background data in the center of small ranges (or windows) and then slides in overlapping steps along the x-axis. Finally, the evaluated background in each center bin is stitched together to form the final background.

The chosen fit function and size of the sliding window are the ones that give the best fit performance. The uncertainties of the background are due to the choice of fit function and on the statistical uncertainty of the data [5].

In the search Ref. [4], two different fit functions were used, depending on which function yielded the best fit performance over the whole invariant mass range. The function used for $|y*| < 0.6$ was,

$$f(x) = p_1(1-x)^{p_2} x^{p_3 + p_4 \ln(x) + p_5 \ln(x^2)} \tag{3.5}$$

where $p_{1,2,3,4,5}$ are fit parameters and where x is defined as $\frac{m_{jj}}{\sqrt{s}}$. The function used for $|y*| < 0.3$ was,

$$f(x) = p_1(1-x)^{p_2} x^{p_3 + p_4 \ln(x)} \tag{3.6}$$

In the search Ref. [5], the following function was used,

$$f(x) = p_1(1-x)^{p_2} x^{p_3} x^{p_4 \log x} \tag{3.7}$$

Statistical Analysis

The p- and z- value are used to see if an excess in the data above the background is significant enough to be a discovery. The p-value can be described as the probability of finding a deviation at least as big as the one observed in the data when doing multiple experiments in absence of signal [33]. The p-value can be translated to a z-value, which is the deviation on the right side of the mean of a Gaussian distribution, in units of standard derivations. They have the relation [33],

$$p - value = \int_z^\infty \frac{1}{\sqrt{2\pi}} e^{-\frac{x^2}{2}} dx \tag{3.8}$$

where p-values ≥ 0.5 correspond to negative z-values. Below this value the relationship between the p- and z- value does not hold. The larger the z- value, and the smaller the p-value, the less probable and more interesting the outcome. Deviations larger than z-values ≥ 3 are considered significant [6]. The p-value depends on what statistical distribution the number of entries in each bin is consistent with. Here, and in most experimental physics studies where the distribution of entries is random, the data is assumed to follow the Poisson distribution, which is the same at the Gaussian distribution if the number of data is large enough [33].

Visualizing the data and the background

The method used in the Jupyter Notebook is walked through to explain the visualization method of data and background used in Ref. [4] and Ref. [5]. The used data was imported from the HEPData, Ref. [34] and Ref. [35], for Ref. [4] and Ref. [5] respectively. The method used to quantify the excess in the papers, using a BumpHunter algorithm, is also described below.

The data set contained the bin edges and center (HIGH, LOW, and mean) for each bin, the number of events/bin, the background data, and the values of the error bars for the fit function and fit parameters of the background. The error bars used for the measured number of events/bin used was $\sqrt{N}$, where N is the number of events.

Different methods can be used to visualize if a deviation between the data and the expectation is significant enough. Several methods were tested, as some methods can leave out or exaggerate significant observations. Two methods were used, the relative distance and the statistical significance with cut, to find significant excesses. These were calculated bin-by-bin. The relative difference is,

$$rel = \frac{D - B}{B} \tag{3.9}$$

where D is the measured data and B is the background data.

The statistical significance was calculated bin-by-bin using the Poisson p-value, with the method shown in Ref. [6]. All the values with p ≥ 0.5 were not shown.

Finally, the measured data were plotted with error bars $\sqrt{N}$ and the background. The significance histograms and the relative difference were plotted in separate diagrams below, see Fig. 3.5 and Fig. 3.7

In the two searches, a BumpHunter algorithm was used to search for a significant bump after visualizing the data. A BumpHunter algorithm compares the invariant mass distribution with the background to search for the most significant bump. The algorithm computes the p-value for different intervals and the bump with the most significant (smallest) p-value is marked [5], [41].

Limit setting phase

Neither search found a bump above the background in the invariant dijet mass distribution. Therefore, the papers could constrain the existence of new particles that couple to quarks, like dark matter mediators such as the Z' boson, when using the mass ranges, luminosities and trigger levels mentioned above.

3.3.3 Results from the Jupyter notebook

The results from the two papers could be reproduced. The plots from Ref. [4] and Ref. [5] along with the same data-sets plotted using the Jupyter Notebook Ref. [6] are displayed below. The significance of the bumps found by the BumpHunter was below 2 for all plots and no discovery was found.

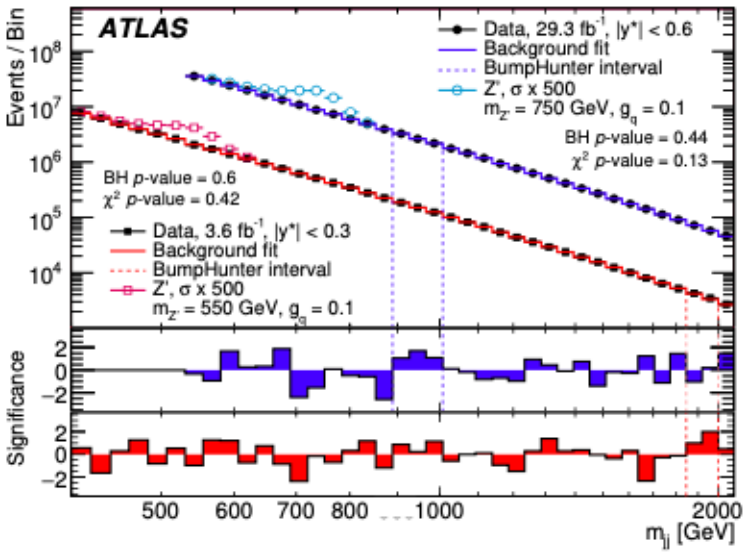

Figure 3.4: Plotted data from search Ref. [4]. Vertical dashed lines indicate the most significant bump found by the BumpHunter algorithm. The significance is displayed below the main plot.

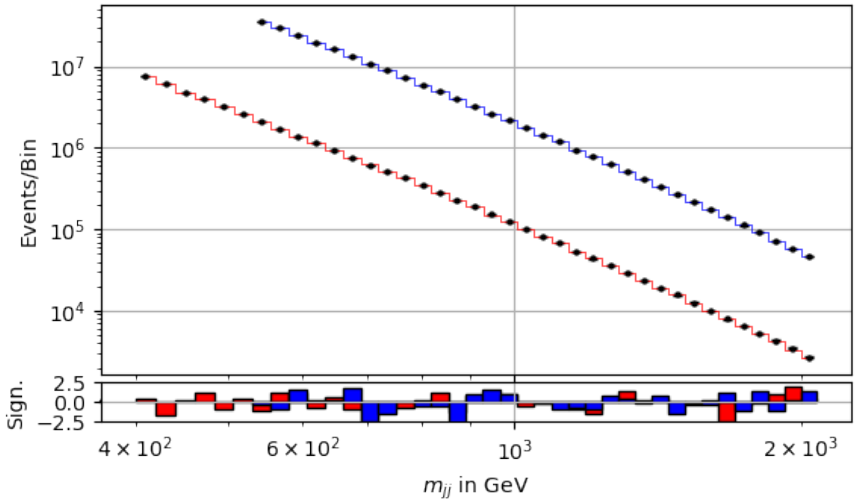

Figure 3.5: Data from the search Ref. [4] plotted using the Jupyter Notebook [6]. The significance is displayed below the main plot.

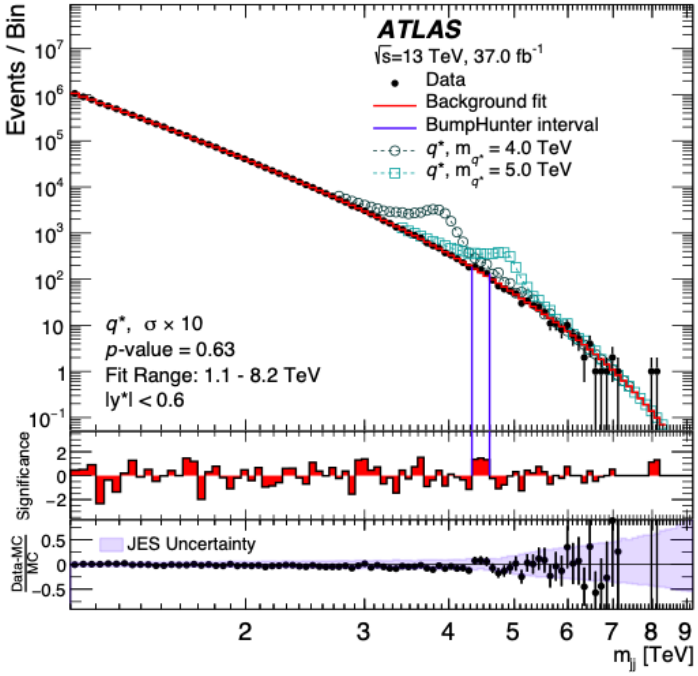

Figure 3.6: Plotted data from search Ref. [5]. Vertical dashed lines indicates the most significant bump found by the BumpHunter algorithm. The significance is displayed below the main plot.

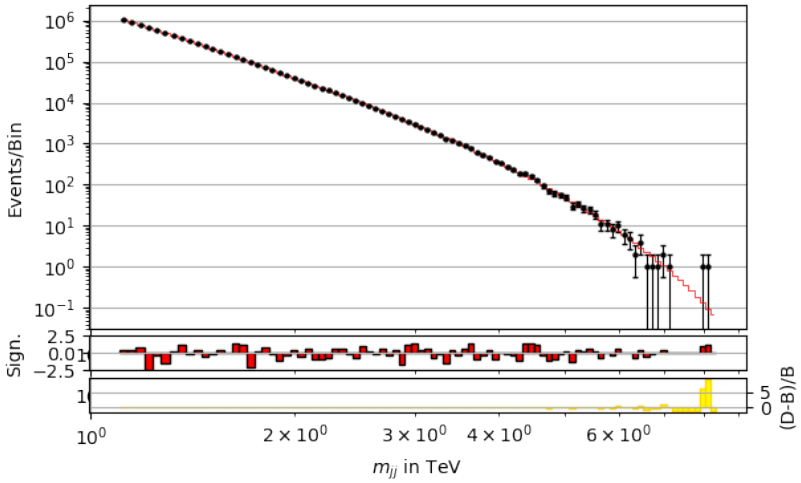

Figure 3.7: Data from the search Ref. [5] plotted using the Jupyter Notebook [6]. The significance is displayed below the main plot.

Chapter 4

LDMX

4.1 The LDMX Experiment

During the upcoming years, the Light Dark Matter eXperiment - LDMX - is planned to be built at SLAC at Stanford [3]. LDMX will search for LDM trough producing dark photons [3]. As mentioned in section 2.3, in the dark photon model, LDM is a thermal relic with the dark photon as a force mediator of SM and DM particles. This search is motivated as thermal relic DM can equally exist in the MeV - GeV mass range as in the TeV mass range.

The LDMX experiment will be a fixed target experiment. To search for dark photons, an electron beam with energy in the GeV range will be aimed at a fixed tungsten target. The electron may change trajectory when interacting with nuclei in the target, which can lead to the emission of a dark photon via a process analogous to bremsstrahlung. If a dark photon is produced, there would be a large missing energy and the electron would have a large transverse momentum, p_T, as the mediator would escape the detector and carry most of the energy. There would also be a lack of other activity in the detector [3].

To get a high resolution, meaning that each electron is measured individually, the beam will consist of 10^8 single and equally spaced electrons/second and a large beam spot will be used. Many collision events and hence a high bunch repetition rate (approximately 40 MHz) are needed as LDMX will be searching for rare events [3].

LDMX will be able to reach regions of parameter space that no other experiment has access to. In particular, LDMX will be able to test interaction strengths below what is required for the relic density, meaning an overproduction of DM in the early universe. Through testing this, the existence of a thermal relic DM with the respective mass within the assumed model can be excluded if not found [42].

LDMX will run in two phases, where the number of electrons per target (EOT), the luminosity, and the energy will vary. In phase two, even lower interaction strengths can be reached [24], [3].

Phase one

- 4×10^{14} EOT
- $L_{int} = 0.8$ pb^{-1}
- Beam with an energy of 4 GeV

Phase two

- 10^{16} EOT
- $L_{int} = 20$ pb^{-1}
- Beam with an energy of 8 - 20 GeV

4.2 LDMX layout

The LDMX experiment will consist of a target, magnet, tagging tracker, recoil tracker, and an E- and HCal, seen in Fig. 4.1 [42]. Many of the detector systems are designed following already existing implementations in other experiments.

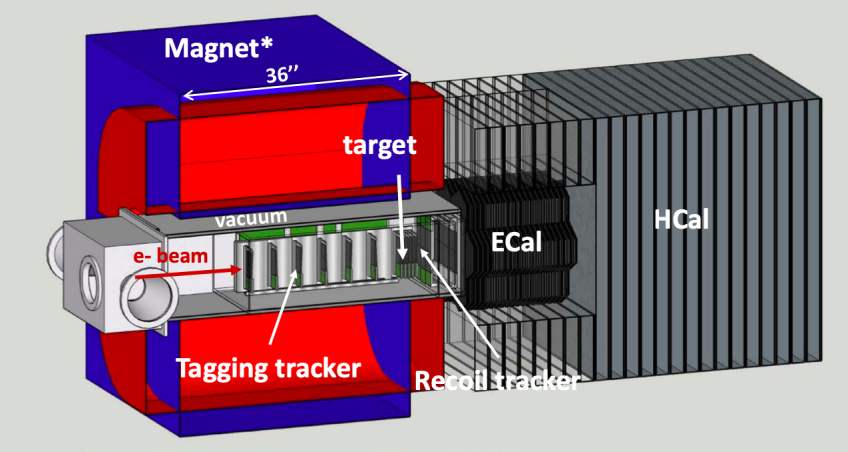

Figure 4.1: Overview of the LDMX experiment layout [43].

The target will consist of a tungsten foil of the dimensions 3 x 8 cm and thickness 350μm, and can easily be varied if needed. A thin target is needed when searching for light DM, as it makes it easier to separate the momentum between reactions. In a thick target, multiple scattering can occur, which deteriorates the momentum resolution [42].

The dipole magnet will have a magnetic field of 1.5 T, to bend the incoming electron's trajectory to measure their momentum [42].

The tagging and recoil tracker will measure the electrons before and after the target respectively. The tagging tracker tags the electron beams with full energy and momentum and the recoil tracker will select recoiled electrons with high transverse momentum [3]. The HCal will consist of a plastic scintillator as an active material, and steel as absorber material. The Ecal will be surrounded by the HCal and consist of silicon and tungsten [42]. As there will be several electrons hitting the target at the same time in phase 2, a high radiation tolerant and high granularity ECal is needed to separate the showers.

The trigger level at LDMX will select events with at least an energy of 2.5 GeV missing [42].

4.3 Background Events

As LDMX will search for one specific type of event, possibly occurring background events can be identified and rejected. Fig. 4.2 is a schematic sketch of the searched dark photon event. The main background, as well an example of a background event that can lead to misleading result, will be discussed below. Current studies show that at least for phase one, all of the difficult backgrounds are expected to be rejected. [42]

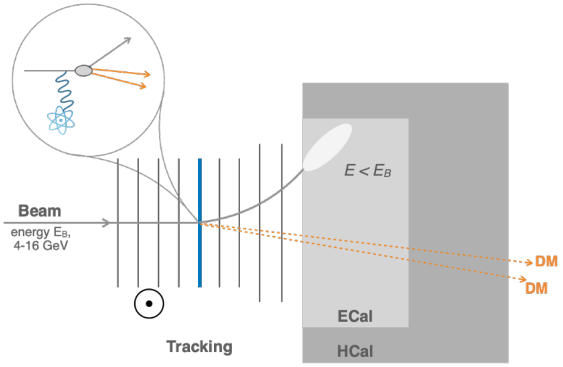

Figure 4.2: A sketch of a produced dark photon decay to LDM at LDMX [42].

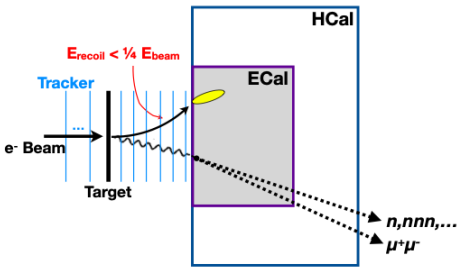

Figure 4.3: A sketch of a produced photo-nuclear event at LDMX [21].

The main background, if a dark photon is not produced, will consist of Bremsstrahlung. These photons will typically leave an electromagnetic shower in the ECal. There will be no missing energy and the electrons and photons will make up the full beam energy. Such events are therefor easy to reject [42].

A background event that can lead to misleading results is if a photon undergoes a photo-nuclear reaction in the target or ECal. [3] A photo-nuclear reaction is when a photon is absorbed by a nucleus, and constituents of the nucleus are ejected [44]. Other particles, for example mesons, can also be produced. In Fig. 4.3 and Fig. 4.1 the similarity of a photo-nuclear and a dark photon event can be seen. A large fraction of photo-nuclear events can be rejected using signals in the ECal. However, there are cases, for example when only neutrons are produced in the photo-nuclear reaction, when nothing is seen in the ECal. Here, the HCal can detect the neutrons and avoid a fake signal event [42].

Chapter 5

Conclusion

From studies of spiral galaxies and galaxy clusters, it is concluded that there has to exist non-visible mass for the movement generated by gravity to hold. From the use of microlensing and studies of the early universe, it has been concluded that this missing mass is not baryonic and makes up 27% of the matter-energy in the universe. Understanding what DM is would be an important addition to our understanding of the universe. If DM is a new particle, it could also help explain other physics phenomena and encourage further developments in the experimental and theoretical fields of particle physics.

There are theoretical models for what DM is hypothesized to be, and experiments search for these models using different experimental designs and characteristics. A collider experiment (ATLAS) and a fixed target experiment (LDMX) were a focus of this thesis. Both experiments search for thermal relic DM. Because thermal relic DM can exist in any mass range, depending on which model is used, both light and massive DM need to be studied. The ATLAS and LDMX experiments and the searches described in this thesis search for mediators decaying to DM, which might not be enough to describe the full complexity of DM.

LDMX, for its first phase, will focus on searching for the invisible decays of the dark photon model. In ATLAS, different kinds of searches are carried out and fewer assumptions are placed on the theoretical models, which increases the spectra for which DM can exist. To produce a Z' boson mediator, ATLAS uses data from high energy proton beams with a total energy of $\sqrt{s} = 13$ TeV, as the mediator is relatively heavy. Mediator masses in the GeV range are difficult to target at ATLAS, as the events cannot be selected effectively, especially for dijet final states, due to the high backgrounds. To produce a dark photon in the GeV range, LDMX will use an intense electron beam, which makes it possible to produce rare, low mass events. Using this, LDMX will be sensitive to lower SM-dark photon interaction strengths than what has been reached before.

ATLAS use 3 orders higher luminosities than the searches at LDMX. Because ATLAS and LDMX are two different experiments, the luminosity is not completely comparable, other than that it shows that the number of interactions that need to be handled by the detector is much higher at ATLAS.

To detect the produced particles, ATLAS and LDMX have similar layouts. Both use a tracking chamber, an ECal and an HCal to detect events, and a trigger level system to select events. The trigger system in ATLAS needs to be more advanced than in LDMX,

as different events are searched for and as the main difficulty at ATLAS is the huge amount of data. To search for a signal that could be DM, both experiments look for missing transverse momenta. At LDMX, the backgrounds can be rejected, while in the dijet searches at ATLAS, the background is irreducible and instead plotted with the data.

In this thesis, two ATLAS papers were also compared.

As discussed in section 3.3 of this thesis, both studies, Ref. [4] and Ref. [5], used pp - collisions at the same center of mass energy of $\sqrt{13}$ TeV and searched for dijet resonances, which could be due to the particles that mediate the interaction between DM and SM. The searches studied different mediator mass ranges, 450 GeV - 1800 GeV in Ref. [4] and 2-9 TeV in Ref. [5]. In Ref. [4], a new trigger level analysis technique was used to make the event sizes smaller and save data storage. This made it possible to store and study more data in the lower mass spectra. With this exception, both papers used the same L1 and HLT trigger system but with different event selections. As Ref. [4] searched for DM particles in lower mass ranges than in Ref. [5], lower p_T trigger thresholds for the leading jet were used in Ref. [4]. The integrated luminosity in Ref. [5] was also higher compared to Ref. [4]. Both papers set constraints on the mass and cross-section on the Z' boson, in different parts of the parameter space. Using the Jupyter Notebook, Ref. [6], the data sets from both searches could successfully be re-plotted.

In the future, LDMX will achieve even lower interaction strengths in phase two, and ATLAS is expected to deliver up to 10 times more data than today by 2026. If a DM candidate were to be found, comparison with indirect and direct DM experiments would be interesting to make.

References

[1] Cern. Dark matter (2020). URL https://home.cern/science/physics/dark-matter.

[2] Cern. Atlas (2020). URL https://home.cern/science/experiments/atlas.

[3] Åkesson, T. *et al.* Light dark matter experiment (ldmx) (2018). 1808.05219.

[4] The ATLAS Collaboration. Search for low-mass dijet resonances using trigger-level jets with the ATLAS detector in pp collisions at $\sqrt{s} = 13$ TeV. *Phys. Rev. Lett.* **121**, 081801 (2018). 1804.03496.

[5] Aaboud, M. *et al.* Search for new phenomena in dijet events using 37 fb^{-1} of pp collision data collected at $\sqrt{s}$ =13 TeV with the ATLAS detector. *Phys. Rev.* **D96**, 052004 (2017). 1703.09127.

[6] Leonie Hermann. A proof-of-principle jupyter notebook using atlas dijet data (2018). URL https://github.com/urania277/jupyter-dijets/blob/master/ProofofPrincipleNotebook_v1.ipynb.

[7] Martin, B. & Shaw, G. *Particle Physics.* Manchester Physics Series (Wiley, 2008), 3 edn.

[8] Cern. Quantum field theory and the electroweak standard model. URL https://cds.cern.ch/record/2315477/plots.

[9] SuperCDMS group. Dark matter. URL https://cdms.phy.queensu.ca/Public_Docs/DM_Intro.html.

[10] Bergström, L. Dark matter: Past, present and future (2015). URL http://indico.ictp.it/event/a14282/session/98/contribution/549/material/slides/0.pdf.

[11] NASA. Looking through a giant magnifying glass (2019). URL https://hubblesite.org/contents/articles/gravitational-lensing.

[12] Universe today. Astronomers figure out how to use gravitational lensing to measure the mass of white dwarfs. URL https://www.universetoday.com/138832/astronomers-figure-use-gravitational-lensing-measure-mass-white-dwarfs/.

[13] Duda, K. G. . G. Modern understanding and evidence. URL https://ned.ipac.caltech.edu/level5/March10/Garrett/Garrett3.html.

[14] Nemiroff, R. & Bonnell, J. Astronomy picture of the day (2006). URL https://apod.nasa.gov/apod/ap060824.html.

[15] Eriksen, H. K. An introduction to the cmb power spectrum (2011). URL http://folk.uio.no/hke/AST5220/v11/AST5220_2_2011.pdf.

[16] Filippini, J. The cosmic microwave background (2005). URL http://cosmology.berkeley.edu/Education/CosmologyEssays/The_Cosmic_Microwave_Background.html.

[17] ESA. Plank and the cosmic microwave background. URL https://www.esa.int/Science_Exploration/Space_Science/Planck/Planck_and_the_cosmic_microwave_background.

[18] Narimani, A. Freeze-out of particles (2016). URL http://www.th.physik.uni-bonn.de/drees/non_ac/presentation_Narimani.pdf.

[19] Chris Mihos. Dark matter - hot and cold (2018). URL http://burro.case.edu/Academics/Astr222/Cosmo/Structure/darkmatter.html.

[20] BERKELY LAB. Cmb simulations at scale (2017). URL https://crd.lbl.gov/departments/computational-science/c3/c3-research/cosmic-microwave-background/cmb-simulations-at-scale/.

[21] Ruth Pöttgen. private communication (2020).

[22] Cern. Atlas explores the dark side of matter (2016). URL http://cerncourier.com/cws/article/cern/65017.

[23] Kim Griest . Thermal relics as dark matter (wimps) (1996). URL http://web.mit.edu/~redingtn/www/netadv/specr/345/node2.html.

[24] Mans, J. The ldmx experiment (2017). URL https://www.epj-conferences.org/articles/epjconf/pdf/2017/11/epjconf_admpp2017_01020.pdf.

[25] CERN. Supersymmetry (2020). URL https://home.cern/science/physics/supersymmetry.

[26] Fairbairn, M., Heal, J., Kahlhoefer, F. & Tunney, P. Constraints on Z' models from LHC dijet searches and implications for dark matter. *JHEP* **09**, 018 (2016). 1605.07940.

[27] Matthew Buckley. Paper explainer: Hiding thermal dark matter with leptons (2017). URL http://www.physicsmatt.com/blog/2017/5/13/paper-explainer-hiding-thermal-dark-matter-with-leptons.

[28] SLAC. Three ways to bust ghostly dark matter (2016). URL https://www6.slac.stanford.edu/files/darkmatter_listicle_formatted_v10.pdf.

[29] Caterina Doglioni, D. T. Searching for dark matter with the atlas detector (2019). URL https://crd.lbl.gov/departments/computational-science/c3/c3-research/cosmic-microwave-background/cmb-simulations-at-scale/.

[30] The ATLAS Collaboration. A new data-collection method for atlas aids in the hunt for new physics (2018). URL https://atlas.cern/updates/physics-briefing/new-data-collection-method-atlas-aids-hunt-new-physics.

[31] Jönsson, L. *Lectures in Particle physics* (Lund, 2016), 1 edn.

[32] The ATLAS Collaboration. Detector and technology (2020). URL https://atlas.cern/discover/detector.

[33] Choudalakis, G. & Casadei, D. Plotting the differences between data and expectation. *The European Physical Journal Plus* **127** (2012). URL http://dx.doi.org/10.1140/epjp/i2012-12025-y.

[34] The ATLAS collaboration. Search for low-mass dijet resonances using trigger-level jets with the atlas detector in pp collisions at $\sqrt{s}$=13 tev (2019). URL https://www.hepdata.net/record/84597.

[35] The ATLAS collaboration. Search for new phenomena in dijet events using 37 fb^{-1} of pp collision data collected at $\sqrt{s}$=13 tev with the atlas detector (2018). URL https://www.hepdata.net/record/77265.

[36] Cern. Luminosity? Why don't we just say collision rate? (2011). URL https://home.cern/news/opinion/cern/luminosity-why-dont-we-just-say-collision-rate.

[37] Krauss, F. Simple relativistic kinematics (2005). URL http://www.cpt.dur.ac.uk/~krauss/Lectures/QuarksLeptons/Basics/Kin_2.html.

[38] Theodor Christian Herwig. Atlas jet trigger performance in 2016 data (2016). URL https://cds.cern.ch/record/2229226/files/ATL-DAQ-PROC-2016-020.pdf.

[39] Jenni, P., Nessi, M., Nordberg, M. & Smith, K. *ATLAS high-level trigger, data-acquisition and controls: Technical Design Report*. Technical Design Report ATLAS (CERN, Geneva, 2003). URL http://cds.cern.ch/record/616089.

[40] John, I. Summarising constraints on dark matter at the large hadron collider (2017). Student Paper.

[41] Choudalakis, G. On hypothesis testing, trials factor, hypertests and the BumpHunter. In *PHYSTAT 2011* (2011). 1101.0390.

[42] Åkesson, T. *et al.* A High Efficiency Photon Veto for the Light Dark Matter eXperiment. *JHEP* **04**, 003 (2020). 1912.05535.

[43] Bertrand Echenard. The ldmx experiment (2018). URL http://online.kitp.ucsb.edu/online/hepfront-c18/echenard/pdf/Echenard_HEPFront18Conf_KITP.pdf.

[44] Ilya Obodovskiy. Radiation methods of matter composition analysis (2019). URL https://www.sciencedirect.com/topics/physics-and-astronomy/photonuclear-reactions.